DOI: 10.1002/ ((please add manuscript number))
Article type: Research Articles

Sustainable and Flexible Microbrush-Faced Triboelectric Generator for Portable/Wearable Applications

Jeonghwa Jeong, Sangheon Jeon, Xiaoting Ma, Young Woo Kwon, Dong-Myeong Shin, Suck Won Hong**

J. Jeong, S. Jeon, Prof. S. W. Hong.
Department of Optics and Mechatronics Engineering
Department of Cogno-Mechatronics Engineering
College of Nanoscience and Nanotechnology
Pusan National University
Busan 46241, Republic of Korea
E-mail: swhong@pusan.ac.kr (S.W.H.)

X. Ma, Prof. D.-M. Shin
Department of Mechanical Engineering
The University of Hong Kong
Pokfulam 999077, Hong Kong, China
E-mail: dmshin@hku.hk (D.M.S.)

Y. W. Kwon
Department of Nano-fusion Engineering
College of Nanoscience and Nanotechnology
Pusan National University
Busan 46241, Republic of Korea

Keywords: triboelectric nanogenerator, microbrush, bundled microfibers, sustainable nanogenerator, energy harvesting

Triboelectric nanogenerators (TENGs) have been put forward as a state-of-the-art energy scavenging technology for self-powered electronics, but their severe wear and degradation driven by inevitable friction can pose significant durability and sustainability concerns. Here, an array of microfibers is reported that functions as a robust and sustainable TENG in both in-plane sliding and vertical contact-separation modes, with excellent electrical potential as high as 20 V and a high cyclability of 3000. The design flexibility of our microbrush TENG (MB-TENG) on the counter materials facilitates the further improvement of electrical outputs, benefiting numerous applications of human-interactive triboelectrification. Significantly, our MB-TENGs offer sufficient output power for successfully driving a smartwatch as well as an electromyography module. This technology uses a simple and cost-effective manner to provide a robust and reliable monolithic TENG module, which is expected to serve as a promising energy harvesting source for self-powered electronics in the near future.

Internet of Things (IoT) technology is emerging to take an essential role in smart cities, where advanced electronics exchange information without requiring human intervention. Although IoT holds the promise of enriching the lives of humans, the technology is expected to encounter massive power consumption issues from the billions of advanced electronics connected through the network. Endeavors to meet the energy demands have focused on developing alternative powering technology, which harvests the abandoned energy resources in an independent, sustainable, and maintenance-free manner. In particular, devices for mechanical energy harvesting – including piezoelectric and triboelectric nanogenerators (PENGs[1-6] and TENGs[7-14], respectively) – have attracted considerable attention given that mechanical energy is ubiquitous. Indeed, TENGs offer many advantages over conventional energy harvesting technologies, including their light weight, simple fabrication, material selection diversity, and high energy conversion efficiency.[15-17] However, as TENGs are based on the working mechanism of contact electrification and electrostatic induction, the inevitable friction causes severe abrasion between the layer surfaces in the contact area, thereby leading to a significant degradation in output power over the cycles.[18-20] The inherent lower durability and sustainability that originate from the working mechanism seriously influence the competitiveness of TENGs compared with other renewable energy harvesting technologies.[21] Some common working environments in which TENGs will be applied, such as with increased dust, moisture, and temperature, may accelerate the mechanical wear.[22-28] Therefore, TENGs that exhibit robustness and toughness in the process of repetitive mechanical stimuli are needed urgently. Moreover, the minute control of the operating environments of TENGs has expanded their application range in structural configurations with variable surface shapes by adopting unusual contact-electrification mechanisms and the critical effects on specific materials systems.[29] Progress in the robustness and reliability of TENGs has been made using various approaches including noncontact mode,[30,31] rolling structural,[32,33] liquid-solid contact,[34,35] self-recovery,[36,37] and encapsulated TENGs.[38,39] At the same time, an easy and straightforward route to improve the durability of TENGs is the structural design methodology with suitable materials. Brush-type surfaces have been designed to provide stable and reliable contact compared with the monolithic surface under the same elastic load.[40] In a recent report, the millimeter-long fur brush has been presented as a lightweight, soft, and low-wear triboelectric material for intriguing TENGs with high elasticity, improved stability, and relatively high density.[41] Compared with a traditional monolithic design, these brushes offer the following features against the friction: 1) an increased contact area, 2) less contact resistance, 3) high resistance to abrasion, 4) less heat generation, and 5) relatively high resilience. Therefore, a tribosurface modified with brushes is a promising candidate for the contact electrification component of durable TENGs. Herein, we report a robust and reliable new-type TENG featuring a surface built with an array of microfibers by using the intrinsic structural advantages of the brush. The array of microfiber bundles (i.e., 6×6, 36 pin-arrays of bundles) implemented into a supporter displays excellent resilience and flexibility, affording a large contact area without any device failure even at large deformation. Our TENG exhibits remarkable capability for mechanical energy harvesting in separate working modes, including in-plane sliding and vertical contact separation. Human being interactive triboelectrification with our TENG reveals outstanding power generation and durability, suggesting that our TENG can serve as a power source for various handheld electronics.

The microbrush architecture of our microfiber-based TENG (hereafter referred to as MB-TENG) comprises an array of microfiber bundles implanted into a holder with an electrical lead wire, as schematically illustrated in **Figure 1**a. The microfiber bundles (i.e., nylon) were transplanted from commercially available chopped fiber-bundles to the pin grid array sockets (i.e., holder, 3D printed polylactic acid, PLA), in which the electrical contacts were precoated using Ag paste over the surface in the frame structure, as described in Figure 1b. Each bundle of fibers was tightly plugged and fixed to the electrically conductive sockets through the curing of the Ag paste, while the other side of the bundles was secured as free-standing, allowing multiple degrees of freedom within this geometric configuration (Figure 1b). The fully integrated MB-TENG device module employed approximately 1,980 microfibers in a given area (20 × 25 mm^2), as shown in Figure 1c. The surface of an individual microfiber measured by scanning electron microscopy exhibits a rough morphology, facilitating contact electrification by enlarging the effective contact area. As manually counted in Figure 1d, the microfibers in the arrays had a typical average length of ~9-10 mm and an average diameter of ~197.6 µm. Along with the advantageous resilience of the individual microfibers, the presented brush structure possesses excellent mechanical durability in elasticity and flexibility in the operation of the TENG. Thus, the structural novelty enables the MB-TENG to markedly tolerate a wide range of axial deformation (i.e., d_0-d_Δ) by enlarging the contact area against counter materials (Figure 1e); the contact area of a single microfiber bundle with respect to transparent substrates could be visualized under the various axial deformations (Figure S1a, Supporting Information). The representative digital images show an apparent increase in the contact area on both rigid glass and soft polydimethylsiloxane (PDMS) substrates upon an increase in the axial deformation (Figure S1b). Control over the elastic properties of counter materials is a critical factor in engendering a large contact area, with a quantitative analysis revealing a boosted contact area with an increasing deformation up to the highest value of ~17.05 mm^2 for a strain of ~70% (Figure S1c).

The typical mechanical tests for the stress-strain response on the 6×6 pin-array of the microfiber bundles compared with the single microfiber bundle are presented in Figure S2. The array structure of the bundled microfibers represents a ~1.5-fold higher maximum compressive stress compared with the single pin-module, and the modulus of resilience calculated from the integration of the stress-strain curve was measured to be E_{array} = 14.9 MN m m^{-3} and E_{single} = 9.5 MN m m^{-3}. In particular, the brush structure did not exhibit any permanent deformation even after the stress was removed. These unique structural properties will greatly benefit the materials design for the triboelectrification effects, and are due largely to the remarkable resilience and flexible nature of the brush structure, which also maximizes the contact area by elastically deforming the shape of the individually arranged microfibers.[42]

The triboelectrification of MB-TENG can be operated by repetitive contacts with the counter materials deposited on the Al electrode (Figure 1f), categorized into two different working modes. First, the nylon in the MB-TENG (i.e., the pins of the microfiber bundles) served as a triboelectrically active material that can be rubbed with the counter materials through the in-plane slide mode. Since nylon is one of the most positive materials in the triboelectric series, its surface generally tends to delocalize electrons while in contact with counter materials. Therefore, when the brush bundle comes into contact with the counter material during the sliding process, an equal quantity of positive and negative charges are symmetrically formed on the surfaces of the brush and counter material, respectively. Once the MB-TENG starts to slide along the surface of the counter materials, the mobile brushes stay above the non-charged region of the stationary counter material. The charge unbalance between the surfaces of the brush and counter material then induces the electrical potential difference between two electrodes, leading to the electron flow through the external circuit. As the MB-TENG continues to slide, the brushes are placed on the charged region of the counter material, and thereby the charge balancing drives the reverse electron flow, which causes an alternating current to the external circuit (Figure S3). The representative output current in contact with the polytetrafluoroethylene (PTFE) film shows 0.88 μA at the sliding speed of 3 m s^{-1} (Figure 1g). The values of the electrically induced charge were calculated from the integration of two single output current peaks, $Q_{polarization}$ = 17.29 nC and $Q_{depolarization}$ = 18.45 nC, indicating that negligible charge loss was observed during sliding. In the second working mode established by the vertical contact-separation process, the compressive and release stimuli drive the periodic electrification between the nylon microbrush and the counter material, resulting in the alternating current (Figure S3). As a representative case, an output current of 0.12 μA was obtained in the contact-separation mode at a compressive load of 70 N (Figure 1h). Indeed, we observed similar polarization and depolarization charges, implying that the electrostatic contribution of the measurement apparatus is negligible.

The main characteristic features in the sliding mode were thoroughly evaluated for the MB-TENG module using a custom measurement setup (**Figure 2**a), in which the initial contact area was precisely controlled to maintain the discontinuous contact between microfibers by adjusting the distance between the MB-TENG and the counter materials (Figure 2b). The MB-TENG was mounted on a fixed support, and the counter material was moved toward the in-plane direction of the MB-TENG using a programmed linear motor, as presented by a real photograph in Figure 2c. In this measurement configuration, we analyzed the electric outputs using an oscilloscope equipped with a current preamplifier. The output voltages generated from the MB-TENG module could be tuned by varying parameters such as initial contact area, sliding speed, and the number of arrays and counter materials. For example, in the case of PTFE counter materials, the results in Figure 2d show an increased output voltage up to the highest value of ~17 V by increasing the contact area (i.e., load-distance) to an enlarged contact area of ~240 mm^2 at a constant sliding speed of 3 m s^{-1}. As reported previously, a slow sliding speed (0.5 m s^{-1}) resulted in the lowest output potential of ~3 V under identical experimental conditions, as an increase in sliding speed gradually boosted output potential (Figure 2e). In this experiment, we found that the electric potential distribution of the MB-TENG was highly dependent on in-plane displacement. The electrification within the physically defined interfaces was computed and visualized as a function of displacement (*D*) using COMSOL Multiphysics as presented in Figure 2f, in which the output voltage reached a maximum of ~4.3 kV for the displacement of 25 mm. Although the electrical potentials from the simulation were much greater than the results obtained from the experiments, which may be likely due to the non-ideal open-circuit condition of the measured output voltages,[43] it is worth noting that an in-plane shift of the microbundle yields the electrical polarization between the MB-TENG and the counter materials. To verify the internal resistance of the MB-TENG, the output voltage and current in contact with the PTFE counter material were investigated using different resistors, as shown in Figure 2g, where the maximum power of 7.96 μW was collected at a load resistance of 0.3 GΩ (Figure S4). The output of a single-bundle MB-TENG module represents ~0.3 V at the initial contact area of ~240 mm^2 at the sliding speed of 3 m s^{-1}, which was a ~55-fold improved result achieved by increasing the number of microfiber bundles up to 36 pillar arrays of bundles, as shown in Figure 2h. This is probably due to the intercalated interaction of each microbrush bundle acting as a charging pump, and thus the output voltage was a constructively integral state when the polarization and depolarization processes from the microfiber bundles were synchronized in the sliding mode. In addition, the long-term stability was rigorously tested for the MB-TENG under the repetitive sliding mode (D = 25 mm). Even after three thousand cycles as shown in Figure 2i, the voltage levels appeared to be stable compared with its initial stage, demonstrating the outstanding durability and robustness of the MB-TENG module. Moreover, by changing the counter materials, the output current and voltage generated in the sliding mode were tested to confirm the versatility of the MB-TENG, as represented in Figure 2j (see also Figure S5). The resulting levels of the output current and voltage on each sample matched well with the trend of the triboelectric series,[44,45] and the surface roughness of counter materials was a critical factor. Sufficient electric output voltage levels from contact with a series of counter materials suggest that our MB-TENG can be applied to portable electronics to conveniently generate triboelectricity, facilitating the friction of rough or apparently smooth surfaces.

Interestingly, we observed that electrical outputs are almost identical when the counter probe was connected with even ground rather than counter electrodes (Figure S6), provisioning the design flexibility as well as an expanded application of our TENG device. We postulated that a new material design concept featuring a single-electrode mode of the MB-TENG would allow the use of loose fabric counter materials for the limited integration of the electrode, as schematically outlined in Figure 2k. When the MB-TENG was slid on four different fabrics – wool, silk, polyvinyl acetate (PVAc), and cotton fibers – the measured results of the output voltage and current at constant sliding speed increased with the increasing electron affinity of the counter materials in the triboelectric table, reaching 8.0 V and 0.8 μA for cotton (Figure 2l-m and Figure S7b). Notably, the sidewalls (i.e., ridges and grooves) from the regularly aligned fabrics enhanced the contact area in the sliding mode for effective triboelectrification by interlocking the lateral side of the microfibers in the slightly penetrated configuration of the MB-TENG (the inset in Figure 2k). As a simple demonstration, when the relative humidity was controlled using an ultrasonic humidifier, the electrical output was obviously degraded by increasing the relative humidity from 15% to 55%. It was clear that water layer formation usually results in the depletion of induced charge on the surface of the triboelectric materials (Figure 2n).[46]

The next strategy for triboelectrification was demonstrated by applying the periodic compressive load to the MB-TENG module in a vertical contact-separation mode (**Figure 3**a). A set of spring spacers at the corners were installed between the MB-TENG and the counter materials to retain a gap of ~10 mm when released from the engaged compressive load. The assembled MB-TENG was placed on the digital scale, and the strain of the microfiber bundles was precisely modulated using a programmed linear motor. Similar to the study for a sliding mode, several measurement parameters, including strain and load frequency, altered the electrical outputs by the motions of the compress-release. Figure 3b displays a set of typical output voltage levels in contact separation with the PTFE film linearly increased, with the strain increasing from -10% to -50% and reaching up to 1.2 V at -50% strain as the contact area was enlarged by the external loads. Separately, the output voltages with different frequencies at the applied load of -50 % strain were measured in Figure 3c. The output voltage of 0.3 V was achieved at an initial low frequency of 3 Hz, and the values were increased to 0.4, 0.5, and 1.2 V in the frequency ranges of 4.5, 6, and 7.5 Hz, respectively. In the triboelectrification process, this frequency dependence is not surprising, as the response time of the electron flow through the external circuit may not be sufficient under certain conditions.[7] Thus, at a higher frequency load, the electron flow has a shorter time to be relaxed through the external circuit compared with that at the lower frequency load, and thereby this increases the output voltage and current signals. The electric potential distribution in the repeated contact-separation mode of the MB-TENG in the open-circuit configuration was simulated and visualized according to the contact length (L) using COMSOL, as shown in Figure 3d. As presented, the total surface charges are balanced when two surfaces are in contact with each other. Once two surfaces are then separated, the electric potential can be generated in the vicinity of each surface. Reaching L = 10 mm, the open-circuit voltage can be maximized up to ~300 V, and the maximum power experimentally generated was 46.72 nW at the load of 100 MΩ (Figure S8). Within the given conditions (i.e., 7.5 Hz, 5 mm), the trends of the electrical potentials extracted from the COMSOL simulation were in good agreement with the measured values from the experiments (Figure 3e-f). Beyond the friction of the machine-interactive motion, the feasibility of triboelectrification by human motions can expand the viable applications of the MB-TENGs. Thus, we performed the hand-tapping test on the MB-TENG equipped with the same spring-spacer configuration as demonstrated earlier (Figure S9a). The electrical outputs driven by manual tapping motion were found to be much larger than that induced by a programmed linear motor (i.e., 31.2 V in Figure S9b-c). Moreover, the TENG that consisted of a planar nylon film without the surface-relief structure exhibited a relatively low output performance of 7.7 V, as presented in Figure 3g and Figure S10. As previously reported, when the same material has characteristic features other than a flat shape on the friction surface, the contact area increases, which improves the output performance.[14,47,48] These results imply that our MB-TENG manifests a notable human-interactive energy harvesting device, which represents the maximum output power of 26 μW at 100 MΩ (Figure S9d-e). More importantly, this trait is particularly advantageous given that the brush has long been a portable common tool used for cleaning, grooming, make-up, painting, etc. In this context, a variety of other counter materials were used to obtain more information, which yielded similar or improved electric output characteristics through a hand-tapping operation (Figure S11). In addition, the triboelectric performance was further enhanced by covering the top surface of the frame structure (i.e., holder, PLA) with a triboelectrically negative material (polyvinyl chloride, PVC film) to collect more electrons from the touching hand, as described in Figure S12a. Surprisingly, as shown in Figure 3h, the output voltage and current in the contact with the PTFE film using the MB-TENG module were remarkably boosted up to 1.6 kV and 200 μA, respectively, in which the maximum output power was 76.7 mW at load resistance of 100 MΩ, as summarized in Figure 3i. This strategy revealed a similar trend by applying other commonly used counter materials such as silicone rubber and polyimide film (Figure 3j and Figure S12b).

Figure 4a illustrates a practical demonstration of the MB-TENG for extending our scheme to a human-interactive device module.[49] The typical MB-TENG modules characterized earlier were readily installed at different locations of the human body – including on the hair, clothes, and shoes – to harvest the friction energy driven by arbitrary human motions. In these demonstrations, the electrical output was maximized by selecting and fitting the optimal working mode of the MB-TENG modules as schematically guided in Figure 4b; hair (in-plane sliding), clothes (in-plane sliding), and shoes (vertical contact separation). Such systems provide an efficient platform for portable or wearable energy harvesting where reversible structural flexibility of the TENGs is essential to the operation. Electrical energy collected by the periodic motions either operated the LED arrays or was stored in a lithium-ion battery that powered commercial healthcare devices such as an electromyography (EMG) module or smartwatch, as illustrated in Figure 4c. Figure 4e provides relevant data on the in-plane sliding mode simply by combing long-hair in an axially aligned direction, similar to that measured in the fabric cases (see Figure 2k). Hence, this unusual approach of the MB-TENG successfully acquired an output voltage and current of up to ~150 V and 6 μA, respectively (Figure 4d), which yielded stable power to light up 100 LEDs (Figure 4e). Another form of the MB-TENG was applied to sportswear (i.e., polyester material) through manual rubbing on the woven fabric surface, providing electrical outputs of 70 V and 1 μA (Figure 4f). Moreover, the basic MB-TENG module could be integrated into the midsole of shoes and serve as a wearable device for a self-charging power supply through body movement. The measured electric potentials were ~50 V with a different frequency of 0.45 Hz and 1.7 Hz for walking and running, respectively, as shown in Figure 4g. Overall, we successfully demonstrated the harvesting of sufficient electrical energy by utilizing transformable MB-TENG modules at several body locations. To ensure the storage of the instantaneous triboelectrification, commercial capacitors were used, in which the separate levels from each charging capacitive voltage dramatically increased up to ~6 V within 40 s (1 μF) and ~5 V within 250 s (10 μF), as summarized in Figure 4h; the charged energy was gradually discharged during 200 s due to the inherent characteristics of the capacitor (Figure S13a). As a means to reliably store harvestable energy, the lithium-ion battery (25 mAh) was used and the circuitry was connected with the MB-TENG in the sliding mode, transforming the mechanical movement (i.e., a linear motor for 28 h, Figure S13b) to a power source for small-scale electronic devices. Although the characteristic output degraded by ~2-3 V compared with the initially prepared TENG module (i.e., only degraded 10-15% in performance) after the repeated friction for a long time (i.e., 28 hours), this experiment clearly evidenced the robustness of our MB-TENG device. Relatively, long periodic movement was required at this stage, but the possible wasted mechanical energies could be collected from other possible situations.[15] Similarly, as a simple test for the power-supply capability of the wearable electronic device, the four 10 F capacitors connected in serial (total capacity: 2.5 F) could be charged to 3.7 V, and then used to drive a smartwatch (Figure S13c-d). Moreover, a representative healthcare monitoring device (i.e., EMG module) was also operated using the lithium-ion battery charged by the MB-TENG, as presented in Figure 4i. Here, the flexible EMG module and epidermal electrodes were attached to the forearm, and the signals of the hand gestures of an open palm and clenched fist were recorded and directly transferred to a smartphone (inset in Figure 4i). Our design approach to the sustainable TENG module to illuminate the energy supply implies potential applications in the future for a variety of research fields such as military, robotics, entertainment, and smart healthcare.[50,51]

In summary, we have reported a simple yet efficient microbrush-based device that exhibits outstanding performance as a robust and reliable TENG, with excellent electrical potential as high as ~20 V and high cyclability of ~3000 in both in-plane sliding and vertical contact-separation working modes. The intuitively succinct design and flexibility of the presented MB-TENG enable the adoption of various forms of counter materials, including polymeric, metallic, and woven fabric materials. Moreover, as the brush has long served as a common handheld tool, the manufactured MB-TENG can be further applied to human-interactive triboelectrification to convert the energy of human motions. Importantly, commercially available small electronic devices such as smartwatches and flexible EMG modules can be successfully powered by harvesting and storing electricity from body motions, allowing the MB-TENG to be used as a universal wearable energy source. We envision that the presented MB-TENGs have viable potential in wearable power sources and can serve not only as a portable energy-harvesting device but also as a transducing medium to interpret signals of human activity recognition and motion-sensing; indeed, a systematic study of the sensory system in the microbrush structure is currently underway.

Experimental Section

Fabrication of the microbrush TENG (MB-TENG). The basic structure of the MB-TENG comprises an array of nylon microfiber bundles and a 3D printed PLA supporter. To construct the brush structure, the nylon microfiber bundles were extracted from a commercial toothbrush, and were then planted into the PLA supporter (20 mm x 25 mm), in which the array of aperture with a diameter of ~2 mm and interspace of ~1.14 mm was three-dimensionally printed over the surface. The microfiber bundles were fastened to the array of aperture on the supporter with silver paste. The full device employed a 6x6 array of microfiber bundles in a given area.

Characterization of the electric output performance. A custom-built mechanical test system was constructed with a programmed linear motor (LS Mechapion, APMC-FAL01AM8K) and a sensitive scale. The MB-TENG was mounted on the linear motor to examine the triboelectric performance against the sliding and compressing load. An oscilloscope (Agilent DSO-X-2014A) equipped with a preamplifier (SRS SR-570) was used for low-noise voltage and current measurements while monitoring both the sliding and compressing load to the MB-TENG.

Characterizations. The morphologies of bundled and individual fibers composing the MB-TENG were observed by a scanning electron microscope (ZEISS SUPRA25, 5-10 kV), optical microscope (Olympus BX51), and digital microscope camera (Hayear, HY-2307). The stress-strain response of fiber bundles was measured using a CT texture analyzer (AMETEK Brookfield).

Numerical simulation via COMSOL. To compute the triboelectrification of the microbrush, 2D models of an array of a brush with dimensions of 2 mm diameter and 10 mm length were built in COMSOL Multiphysics, matched with the actual dimensions of the MB-TENG. Vertical displacements from 0 mm to 10 mm and horizontal displacements from 0 mm to 25 mm were introduced to the MB-TENG. For potential distribution simulations with an open-circuit condition, the surface charges of 2 nC and 20 nC were set for nylon fibers at the in-plane sliding and vertical contact-separation modes, respectively. The total charge on the PTFE counter material was set to -2 nC and -20 nC at the in-plane sliding and vertical contact-separation modes, respectively.

Supporting Information

Supporting Information is available from the Wiley Online Library or from the author.

Acknowledgements

J.J. and S.J. contributed equally to this work. This work was supported by the National Research Foundation (NRF) of Korea under the auspices of the Ministry of Science and ICT, Republic of Korea (NRF-2020R1F1A1077033). This research was also supported by a grant of the Korea Health Technology R&D Project through the Korea Health Industry Development Institute (KHIDI), funded by the Ministry of Health & Welfare, Republic of Korea (HI18C2383). X. Ma and Dr. D.-M. Shin acknowledge the financial support of the Early Career Scheme of the Research Grants Council of the Hong Kong Special Administrative Region, China, under Award Number 27202920. Additionally, the authors would like to acknowledge Vicky Geall for editorial assistance.

Received: ((will be filled in by the editorial staff))
Revised: ((will be filled in by the editorial staff))
Published online: ((will be filled in by the editorial staff))

References

[1] Z. L. Wang, J. Song, *Science* **2006**, *312*, 242.
[2] M. Lee, C. Chen, S. Wang, S. N. Cha, Y. J. Park, J. M. Kim, L. Chou, Z. L. Wang, *Adv. Mater.* **2012**, *24*, 1759.
[3] Y. Hu, L. Lin, Y. Zhang, Z. L. Wang, *Adv. Mater* **2012**, *24*, 110.
[4] D. Shin, E. L. Tsege, S. H. Kang, W. Seung, S. Kim, H. K. Kim, S. W. Hong, Y. Hwang, *Nano Energy* **2015**, *12*, 268.
[5] D. Shin, H. J. Han, W. Kim, E. Kim, C. Kim, S. W. Hong, H. K. Kim, J. Oh, Y. Hwang, *Energy Environ. Sci* **2015**, *8*, 3198.
[6] D. Shin, S. W. Hong, Y. Hwang, *Nanomaterials* **2020**, *10*, 123.
[7] F. Fan, Z. Tian, Z. L. Wang, *Nano Energy* **2012**, *1*, 328.
[8] H. Guo, Z. Wen, Y. Zi, M. Yeh, J. Wang, L. Zhu, C. Hu, Z. L. Wang, *Adv. Energy Mater.* **2016**, *6*, 1501593.
[9] T. Jiang, H. Pang, P. Lu, Y. Feng, X. Liang, W. Zhong, Z. L. Wang, *Adv. Energy Mater.* **2020**, *10*, 2000064.
[10] R. Hinchet, H. Yoon, H. Ryu, M. Kim, E. Choi, D. Kim, S. Kim, *Science* **2019**, *365*, 491.
[11] J. Kim, H. Cho, M. Han, Y. Jung, S. S. Kwak, H. Yoon, B. Park, H. Kim, H. Kim, J. Park, S. Kim, *Adv. Energy Mater.* **2020**, *10*, 2002312.
[12] H. Yoon, M. Kang, W. Seung, S. S. Kwak, J. Kim, H. T. Kim, S. Kim, *Adv. Energy Mater.* **2020**, *10*, 2000730.
[13] H. Phan, D. Shin, S. H. Jeon, T. Y. Kang, P. Han, G. H. Kim, H. K. Kim, K. Kim, Y. Hwang, S. W. Hong, *Nano Energy* **2017**, *33*, 476.
[14] T. Kim, S. Jeon, S. Lone, S. J. Doh, D. Shin, H. K. Kim, Y. Hwang, S. W. Hong, *Nano Energy* **2018**, *54*, 209.
[15] C. Wu, A. C. Wang, W. Ding, H. Guo, Z. L. Wang, *Adv. Energy Mater.* **2019**, *9*, 1802906.
[16] Z. L. Wang, *Adv. Energy Mater.* **2020**, *10*, 2000137.

[17] H. Yoon, H. Ryu, S. Kim, *Nano Energy* **2018**, *51*, 270.

[18] K. Parida, V. Kumar, W. Jiangxin, V. Bhavanasi, R. Bendi, P. S. Lee, *Adv. Mater.* **2017**, *29*, 1702181.

[19] J. Sun, X. Pu, M. Liu, A. Yu, C. Du, J. Zhai, W. Hu, Z. L. Wang, *ACS Nano* **2018**, *12*, 6147.

[20] W. Xu, L. Huang, J. Hao, *Nano Energy* **2017**, *40*, 399.

[21] W. Hu, M. Wong, J. Hao, *Nano Energy* **2019**, *55*, 203.

[22] M. A. Chowdhury, M. Helali, *Open Mech. Eng. J.* **2008**, *2*, 128.

[23] W. Ding, J. Zhou, J. Cheng, Z. Wang, H. Guo, C. Wu, S. Xu, Z. Wu, X. Xie, Z. L. Wang, *Adv. Energy Mater.* **2019**, *9*, 1901320.

[24] G. Q. Gu, C. B. Han, C. X. Lu, C. He, T. Jiang, Z. L. Gao, C. J. Li, Z. L. Wang, *ACS Nano* **2017**, *11*, 6211.

[25] E. J. Berger, C. M. Krousgrill, F. Sadeghi, *J. Tribol.* **1997**, *119*, 672.

[26] C. Xu, A. C. Wang, H. Zou, B. Zhang, C. Zhang, Y. Zi, L. Pan, P. Wang, P. Feng, Z. Lin, Z. L. Wang, *Adv. Mater.* **2018**, *30*, 1803968.

[27] A. C. Wang, B. Zhang, C. Xu, H. Zou, Z. Lin, Z. L. Wang, *Adv. Funct. Mater.* **2020**, *32*, 1909384.

[28] C. Xu, B. Zhang, A. C. Wang, H. Zou, G. Liu, W. Ding, C. Wu, M. Ma, P. Feng, Z. Lin, Z. L. Wang, *ACS Nano* **2019**, *13*, 2034.

[29] C. Xu, A. C. Wang, H. Zou, B. Zhang, C. Zhang, Y. Zi, L. Pan, P. Wang, P. Feng, Z. Lin, Z. L. Wang, *Adv. Mater.* **2018**, *30*, 1803968.

[30] L. Lin, S. Wang, S. Niu, C. Liu, Y. Xie, Z. L. Wang, *ACS Appl. Mater. Interfaces* **2014**, *6*, 3031.

[31] J. Chen, J. Yang, H. Guo, Z. Li, L. Zheng, Y. Su, Z. Wen, X. Fan, Z. L. Wang, *ACS Nano* **2015**, *9*, 12334.

[32] H. Yong, J. Chung, D. Choi, D. Jung, M. Cho, S. Lee, *Sci. Rep.* **2016**, *6*, 1.

[33] D. Kim, I. Tcho, Y. Choi, *Nano Energy* **2018**, *52*, 256.

[34] L. Pan, J. Wang, P. Wang, R. Gao, Y. Wang, X. Zhang, J. Zou, Z. L. Wang, *Nano Res.* **2018**, *11*, 4062.

[35] D. Choi, S. Lee, S. M. Park, H. Cho, W. Hwang, D. S. Kim, *Nano Res.* **2015**, *8*, 2481.

[36] W. Xu, L. Huang, J. Hao, *Nano Energy* **2017**, *40*, 399.

[37] Y. Yang, M. W. Urban, *Chem. Soc. Rev.* **2013**, *42*, 7446.

[38] L. Gu, N. Cui, J. Liu, Y. Zheng, S. Bai, Y. Qin, *Nanoscale* **2015**, *7*, 18049.

[39] K. Y. Lee, H. Yoon, T. Jiang, X. Wen, W. Seung, S. Kim, Z. L. Wang, *Adv. Energy Mater.* **2016**, *6*, 1502566.

[40] J. Xiao, L. Liu, C. Zhang, L. Zhang, K. Zhou, *Wear* **2016**, *368*, 461.

[41] P. Chen, J. An, S. Shu, R. Cheng, J. Nie, T. Jiang, Z. L. Wang, *Adv. Energy Mater.* **2021**, 2003066.

[42] R. Lewis, R. S. Dwyer-Joyce, M. J. Pickles, *Wear* **2004**, *257*, 368.

[43] L. Shi, S. Dong, H. Xu, S. Huang, Q. Ye, S. Liu, T. Wu, J. Chen, S. Zhang, S. Li, X. Wang, H. Jin, J. M. Kim, J. Luo, *Nano Energy* **2019**, *64*, 103960.

[44] D. M. Gooding, G. K. Kaufman, *Encyclopedia of Inorganic and Bioinorganic Chemistry*, Wiley, Hoboken, NJ **2011**.

[45] J. W. Lee, B. U. Ye, J. M. Baik, *APL Mater.* **2017**, *5*, 073802.

[46] R. Wen, J. Guo, A. Yu, J. Zhai, Z. L. Wang, *Adv. Funct. Mater.* **2019**, *29*, 1807655.

[47] H. J. Choi, J. H. Lee, J. Jun, T. Y. Kim, S. W. Kim, H. Lee, *Nano Energy* **2016**, *27*, 595.

[48] S. Chun, C. Pang, S. B. Cho, *Adv. Mater.* **2020**, *32*, 1905539.

[49] J. J. P. C. Rodrigues, D. B. D. R. Segundo, H. A. Junqueira, M. H. Sabino, R. M. Prince, J. Al-Muhtadi, V. H. C. D. Albuquerque, *IEEE Access* **2018**, *6*, 13129.

[50] J. Chen, Z. L. Wang, *Joule* **2017**, *1*, 480.

[51] X. Peng, K. Dong, C. Ye, Y. Jiang, S. Zhai, R. Cheng, D. Liu, X. Gao, J. Wang, Z. L. Wang, *Sci. Adv.* **2020**, *6*, eaba9624.

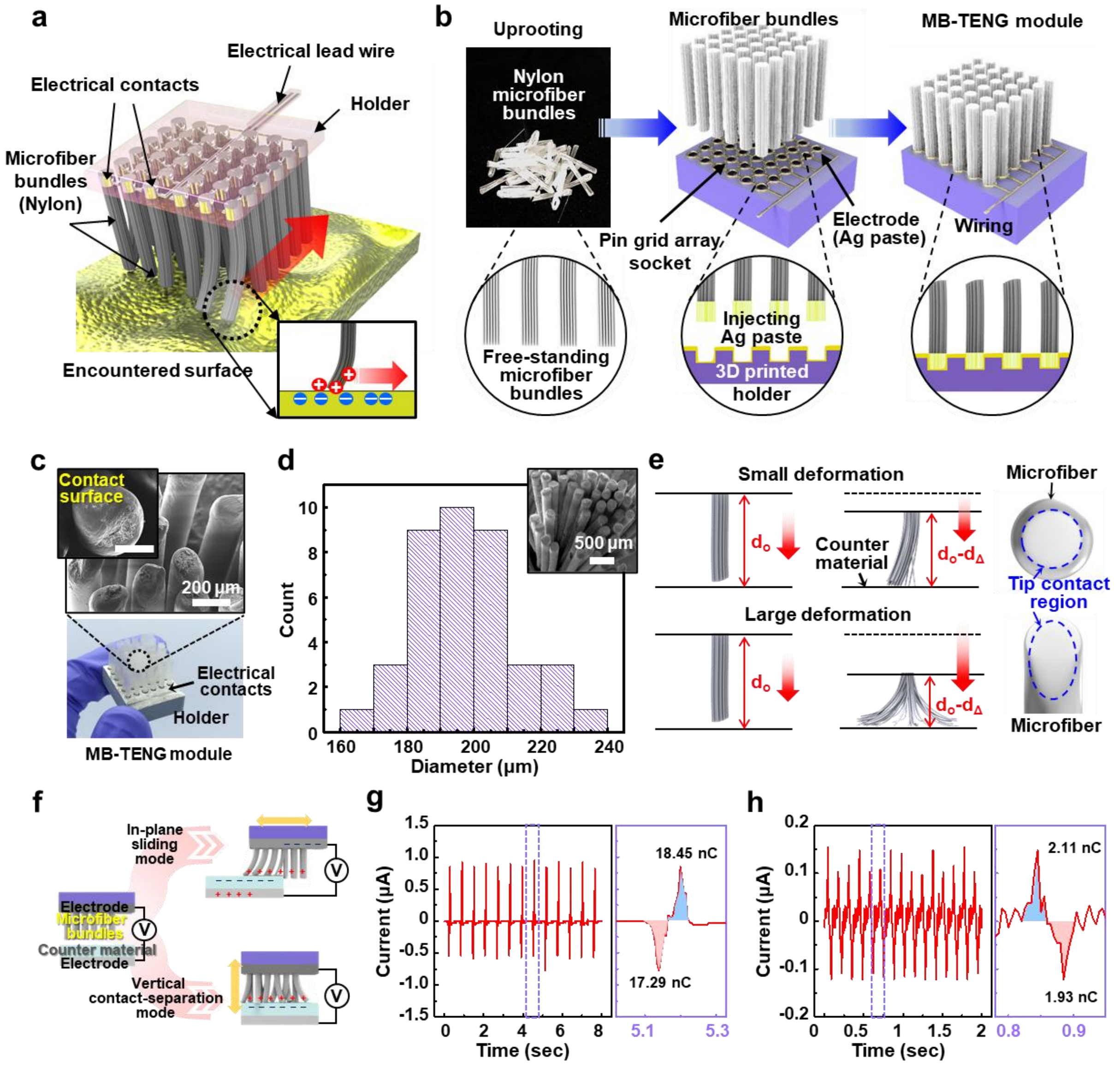

Figure 1 | Concept and design of the MB-TENG-based energy harvesting system. a) Schematic illustration of the MB-TENG component generating triboelectrification. **b)** The fabrication process to produce the MB-TENG utilizing chopped fiber-bundles and a pin grid array socket connected with electrically conductive Ag paste; corresponding cross-sectional images are presented for each manufacturing process (bottom). **c)** Scanning electron microscopy image of the surface morphology in the microfibers (inset: magnified rough surface, scalebar = 100 μm) as a contact area for triboelectrification, and photograph of the fully integrated MB-TENG module (bottom). **d)** A histogram representing the diameter distribution of the bundled microbrushes in the TENG module. **e)** A deflected single microfiber with tip contact at the axis-dependent deformation; the contact region can be defined as an oval shape by the increased contact area. **f)** The MB-TENG integrated with the counter material to enable two different working modes. Representative output current (left) and transferred charge calculated from a current peak (right), where measured in sliding mode, **g)** and in vertical contact-separation mode, **h)**, respectively.

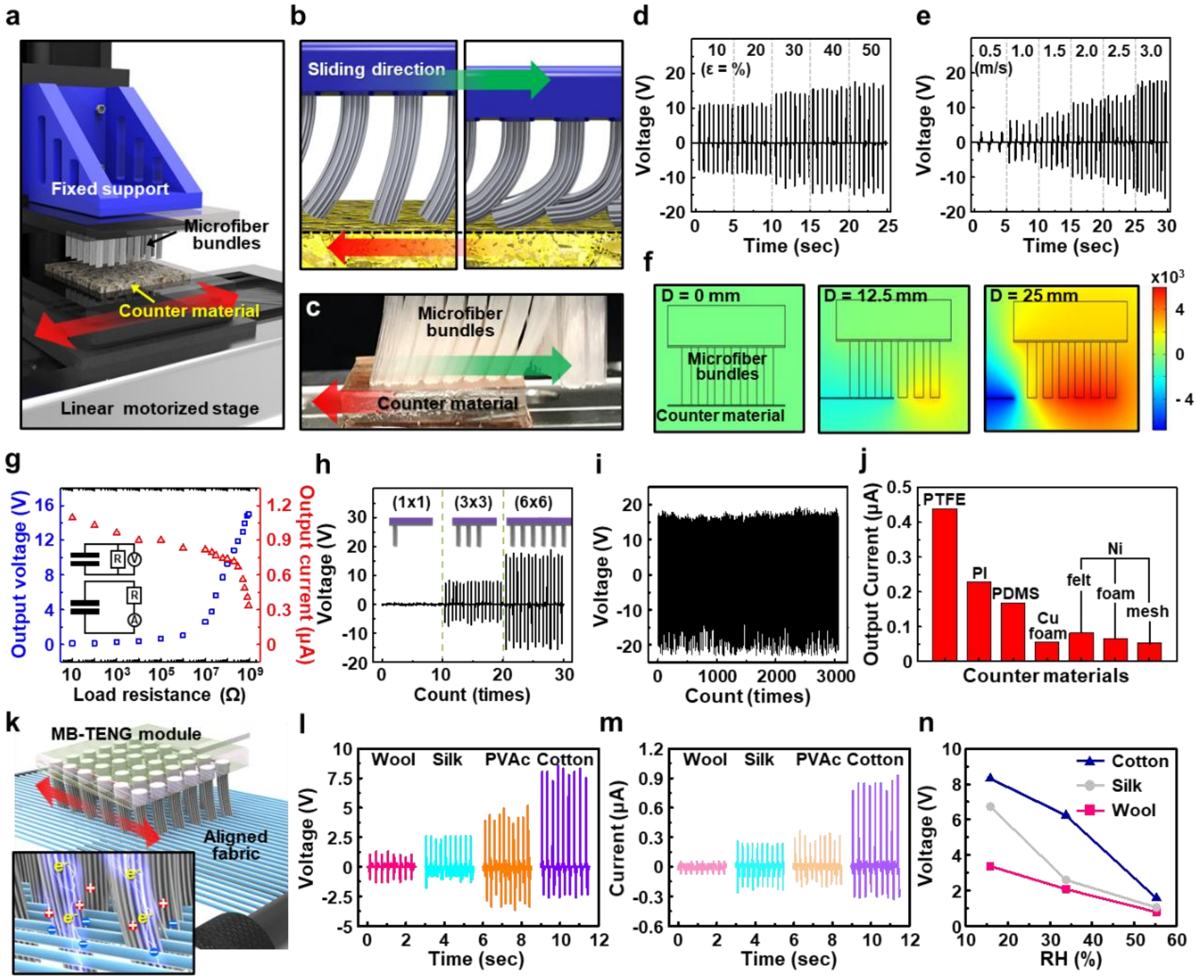

Figure 2 | Characterization of the sliding mode for the MB-TENG. a) Schematic illustration of the measurement setup. **b)** Enlarged side view examples of the sliding mode MB-TENG when contacted with a counter material, representing the capability to slide under the tunable vertical distances. **c)** Real digital image of the MB-TENG equipped in the measurement setup. **d-e)** Output voltage of the typical MB-TENG module under different strains from 10% to 50 % at a sliding speed of 3 m s^{-1} and 50% of strain at different sliding speeds. **f)** COMSOL simulation results of the MB-TENG at different separation distances. **g)** Output characteristics depending on the load resistance. **h)** Each representative output voltage performance with the increase in the number of MBs. **i)** Long-term stability of output voltage during 3000 cyclic motions. **j)** Output current of the MB-TENGs matched with various types of counter materials. **k)** Schematic illustration of the sliding MB-TENG mode on regularly aligned fabrics in the single-electrode mode, enhancing the contact area by interlocking the lateral side of the microfibers (inset). **l-m)** Output voltage and current measured from the sliding MB-TENG on various aligned fabrics. **n)** Measured peak voltage values under different relative humidity from 15% to 55%.

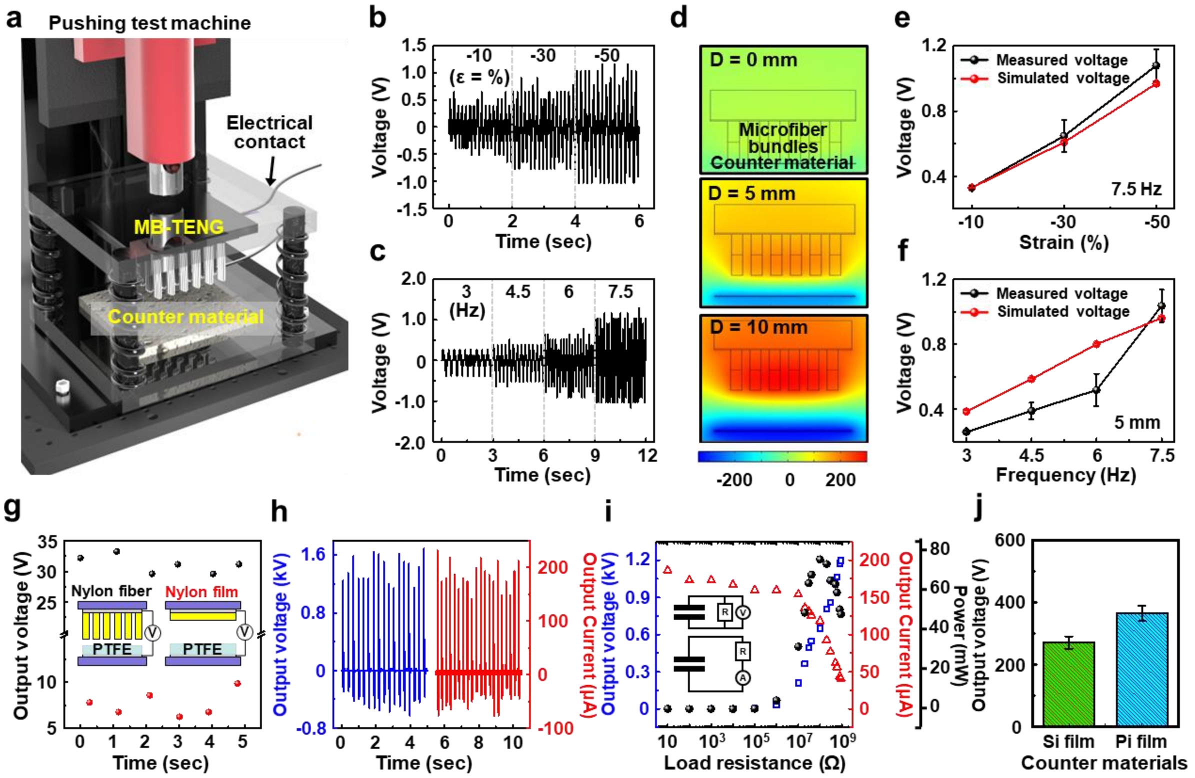

Figure 3 | Characterization of the contact-separation mode for the MB-TENG. a) Schematic illustration of the measurement setup for the contact-separation mode MB-TENG, consisting of a programmed linear motor and the assembled MB-TENG. **b-c)** Output voltage of the MB-TENG under different strains at a 7.5 Hz of frequency and under 50% of the strain at different load frequencies. **d)** COMSOL simulation of the potential distribution in the MB-TENG for the different contact lengths between MBs and the counter material. **e-f)** Computed and experimental results of the potential differences generated by the MB-TENG under the same conditions as b) and c). **g)** Comparison of output voltages of the fiber and film structure TENGs (black dots: nylon fiber, red dots: nylon film). **h)** The output voltage and current of the MB-TENG with PVC film on the top surface of the frame structure. **i)** The output voltage and current of the MB-TENG measured at different external load resistances varying from 10 Ω to 910 MΩ and calculated output power (inset shows a circuit diagram of the measurement system). **j)** Output voltages of MB-TENGs using other counter materials for silicone and polyimide film.

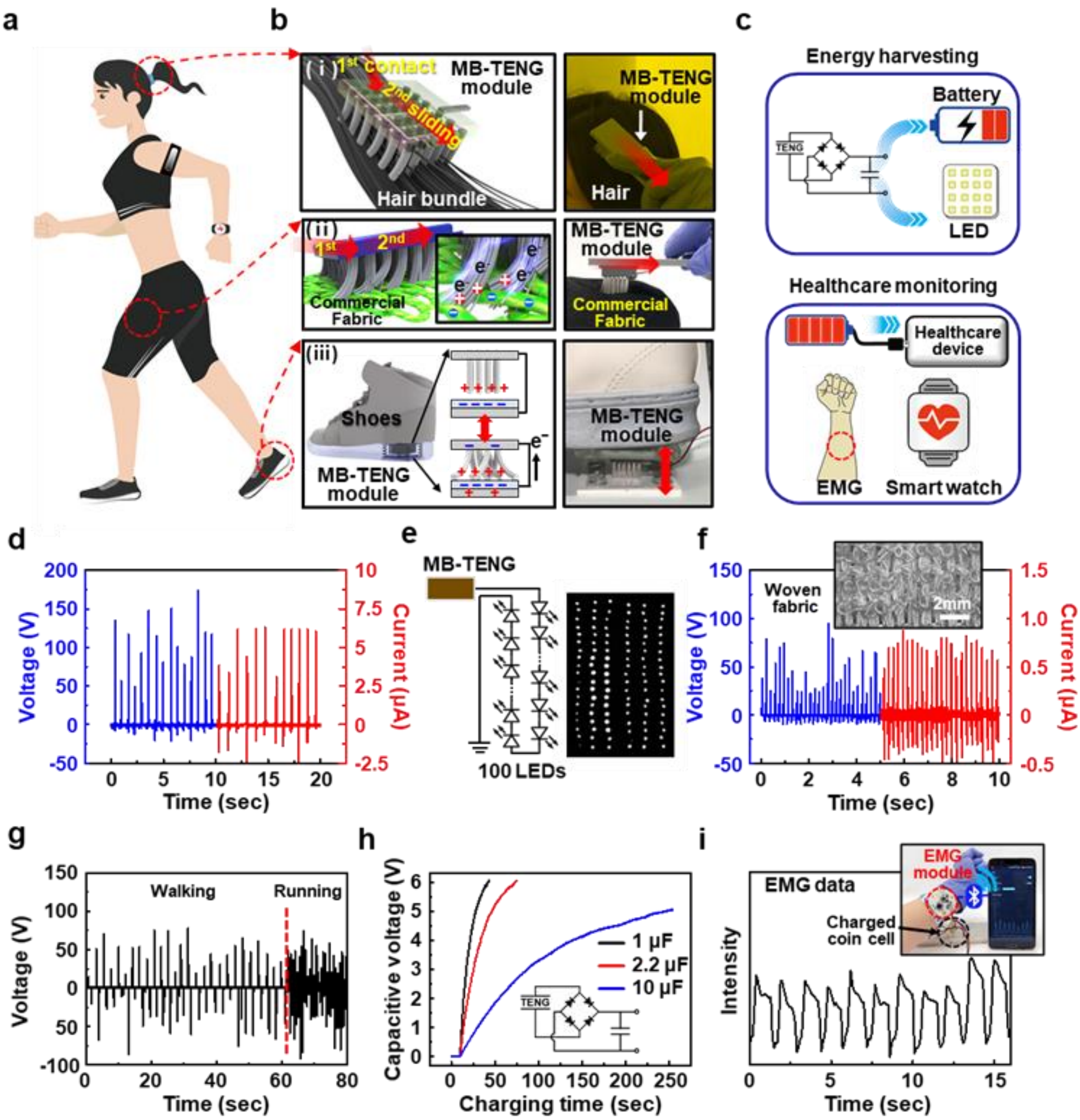

Figure 4 | a) Conceptual illustration of the practical demonstration of the MB-TENGs as a human-interactive device. **b)** Schemes and matched photographs of the MB-TENGs to apply the optimal working modes as (i) combing hair, (ii) sweeping fabrics, and (iii) fixed under a shoe. **c)** Utilization of the harvested energy from the MB-TENGs for lighting up LED arrays, charging a lithium-ion battery, or healthcare monitoring. **d)** Output voltage and current harvested from the case (i). **e)** Circuit diagram for LED arrays connected in a series and actual powering demonstration, lighting up to 100 LEDs. **f)** Output voltage and current measured from the motion of case (ii); the inset shows a photograph of the fabric counter materials. **g)** Output voltage during the process of walking and running with case (iii). **h)** Capacitive charging behavior with hand tapping MB-TENGs; the inset shows a circuit diagram consisting of an MB-TENG and a capacitor. **i)** The measured EMG signals by the continuous hand gestures; the inset shows a photograph of the EMG module and wireless system with a smartphone.

Our microbrush-faced triboelectric nanogenerator featuring high robustness, outstanding sustainability, and excellent durability displays remarkable capability for mechanical energy harvesting in separate working modes. Human being interactive triboelectrification with our device reveals outstanding power generation and durability, suggesting that our device can serve as a power source of various handheld electronics.

Jeonghwa Jeong, Sangheon Jeon, Xiaoting Ma, Young Woo Kwon, Dong-Myeong Shin* and Suck Won Hong*

Sustainable and Flexible Microbrush-Faced Triboelectric Generator for Portable/Wearable Applications

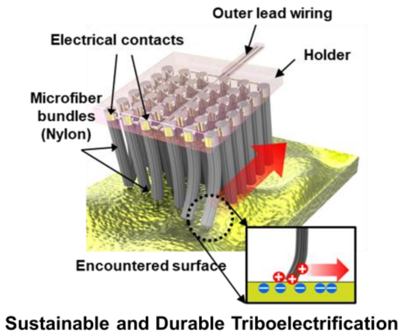

Supporting Information

Sustainable and Flexible Microbrush-Faced Triboelectric Generator for Portable/Wearable Applications

Jeonghwa Jeong, Sangheon Jeon, Xiaoting Ma, Young Woo Kwon, Dong-Myeong Shin and Suck Won Hong**

Supplementary Figures

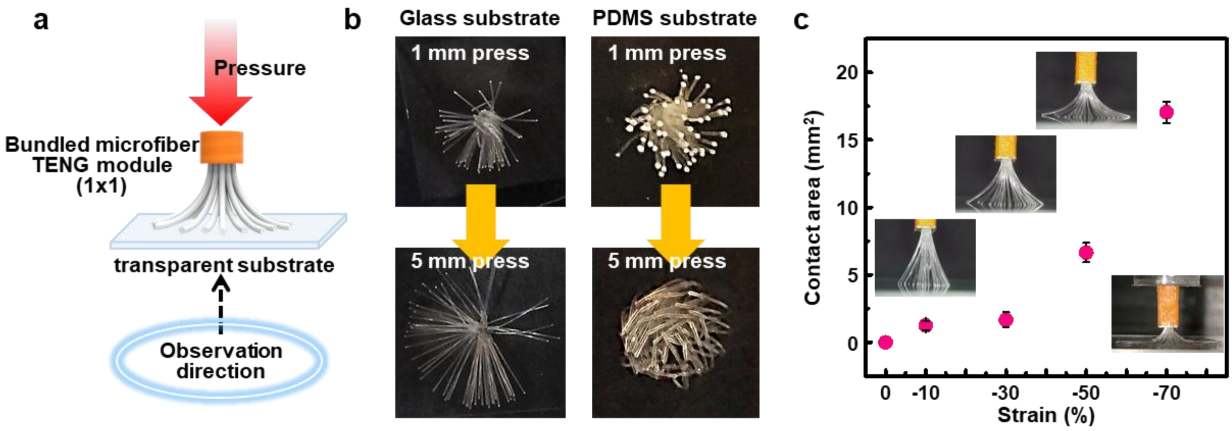

Figure S1. Visualization of the estimated contact area for a single microfiber bundle with respect to various axial deformation. a) A schematic drawing on the direct observation for the contact area of a single microfiber bundle, monitored through a transparent substrate (i.e., smooth glass and tacky PDMS). b) The captured images of the deformed microfibers at 1 mm and 5 mm on each contacted substrate. c) The expanded contact area depending on the fiber-spreading at each axial deformation on a glass substrate.

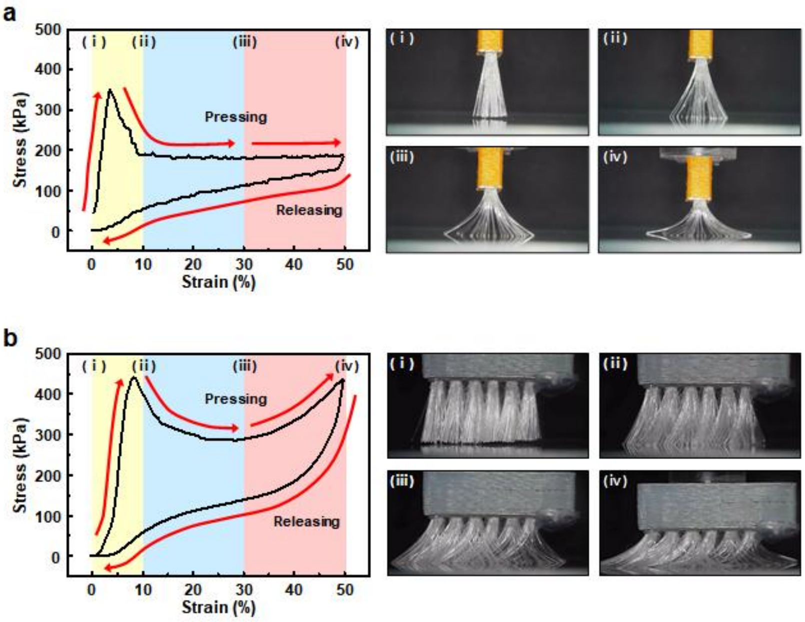

Figure S2. Direct comparison of plastic deformation (i.e., press-to-release) for each TENG module. a-b) The stress-strain graph of a single microfiber bundle and 6×6 pin-array module, respectively. Increased strain from (i) to (ii) regions in the graph reflects the elastic modulus of each TENG module based on the microfiber bundles. For the 6×6 pin-array module in b, the mechanical property at the region (iv) represents the increased stress by the interrupted spread of the microfiber-pin array.

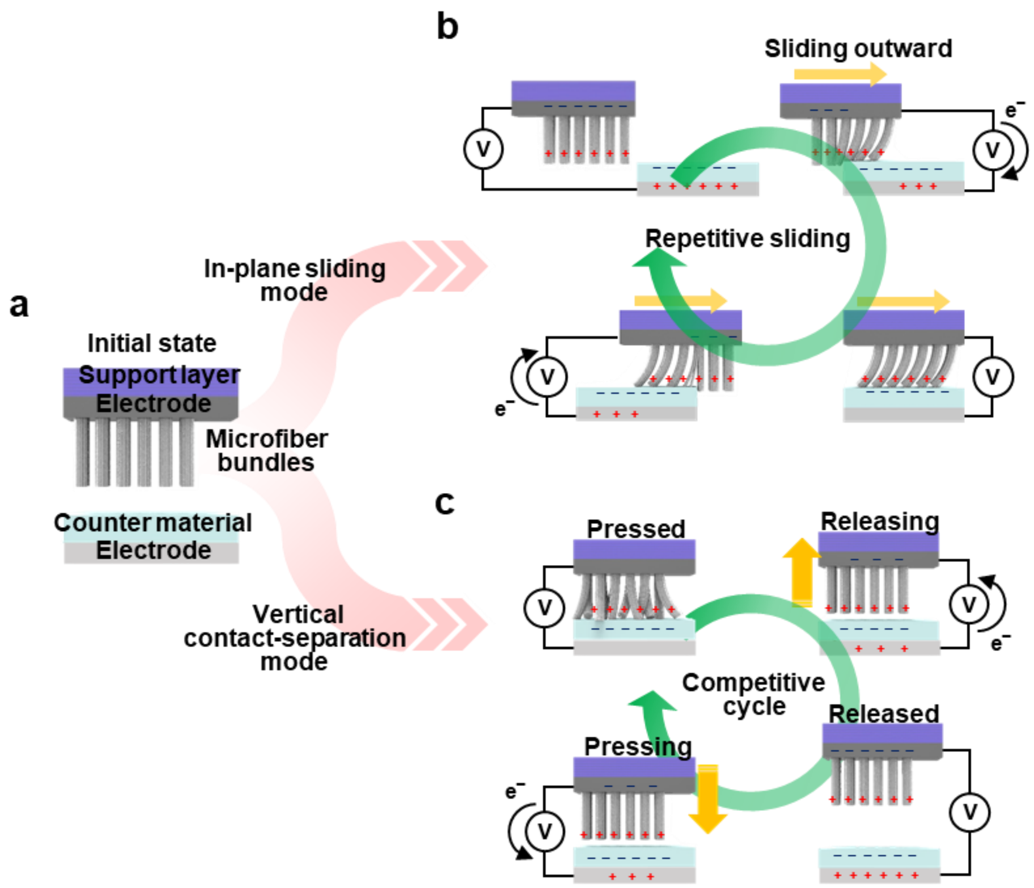

Figure S3. a) The originally designed structure of the MB-TENG. b) The series of schematic illustrations of the related charge transfer mechanism in the sliding mode of TENG when two different substances are contacted under the engaged condition. In the process, the periodic change of the potential difference can be induced on each step between the microbrush and counter materials through the cyclic frictions. When the two materials are facilitated by sliding friction, the negative charges from the counter materials generate the electron flows to the external electrode under a positive charges on the surface of the microbrush. In the following, the charged state is transformed to the initial state when the two surfaces are separated (i.e., released state). Depending on the in-plane sliding distance changes, the triboelectric effect induced by the potential difference (i.e., opposite triboelectric charges on the surface) can be increased. c) The series of schematic illustrations of the related charge transfer mechanism in the contact-separation mode of TENG. Likewise the former case, the potential difference occurs when the two surfaces are repetitively agitated between the frictional charged surfaces; the electrons by the triboelectrification can be driven to flow through the external electrode to the opposite direction. In the two different modes, the shortening of the vertical distance between the tribologically active material and the enlarging of the frictional area of the microfiber can lead to a larger electrical potential.

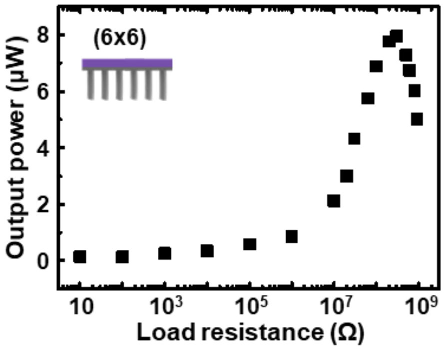

Figure S4. Output power according to the load resistance in the sliding mode (6×6 module) with PTFE counter material, representing the maximum power output of 7.96 μW at load resistance of 3×10^8 Ω.

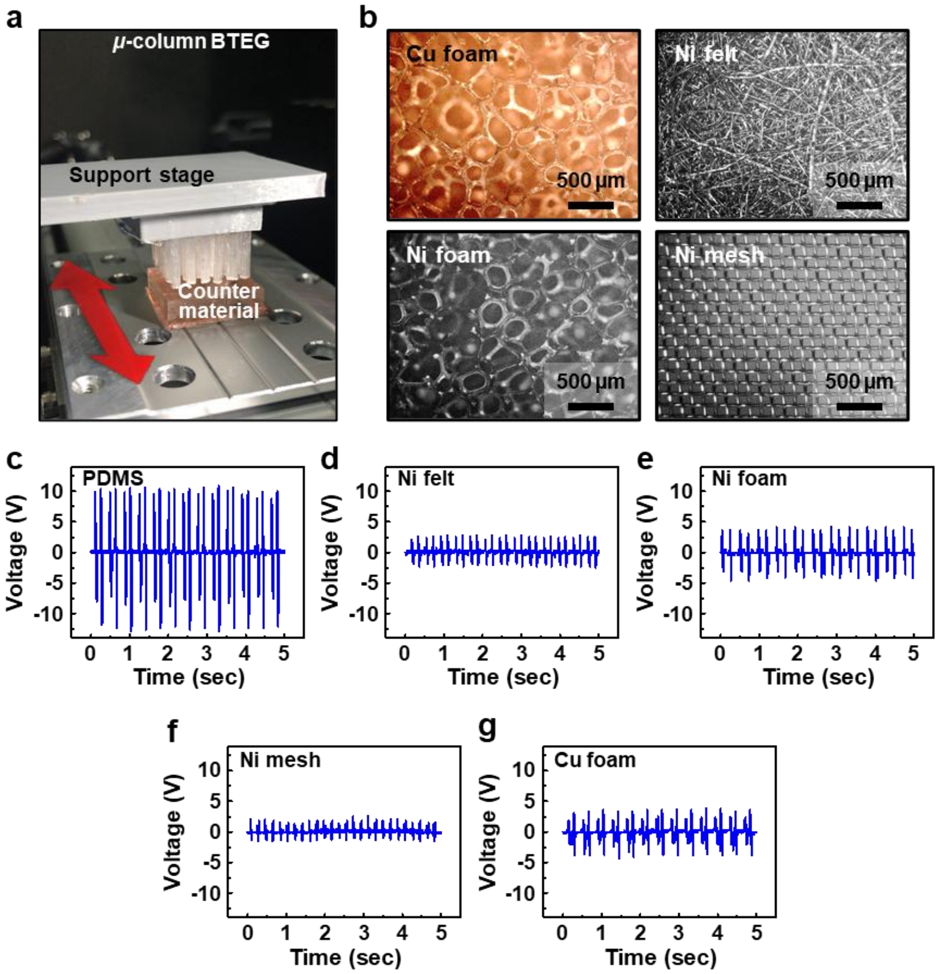

Figure S5. a) Actual operating image during the sliding mode test using a linear motor; the MB-TENG module is fixed to a separate support on the top of the linear motor, and the counter material is attached to the lower stage of the linear motor to move back and forth. b) Microscopic photographs of counter materials with various shapes (i.e., Cu foam, Ni felt, Ni foam, and Ni mesh) used in the test. c-g) Representative output voltages from the sliding mode test with the MB-TENG (i.e., 6×6 module). The levels of the output voltage present in the order of PDMS, Ni foam, and Cu foam, which is in good agreement with the trend of the triboelectric series from the nylon microfiber.

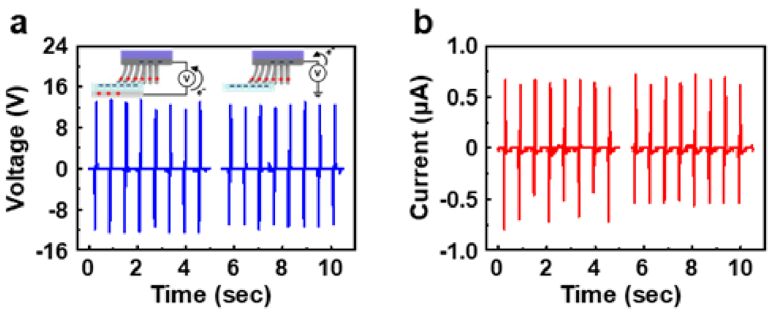

Figure S6. The representative values of the output voltage and current, separately measured in a) sliding and b) single-electrode mode using a linear motor.

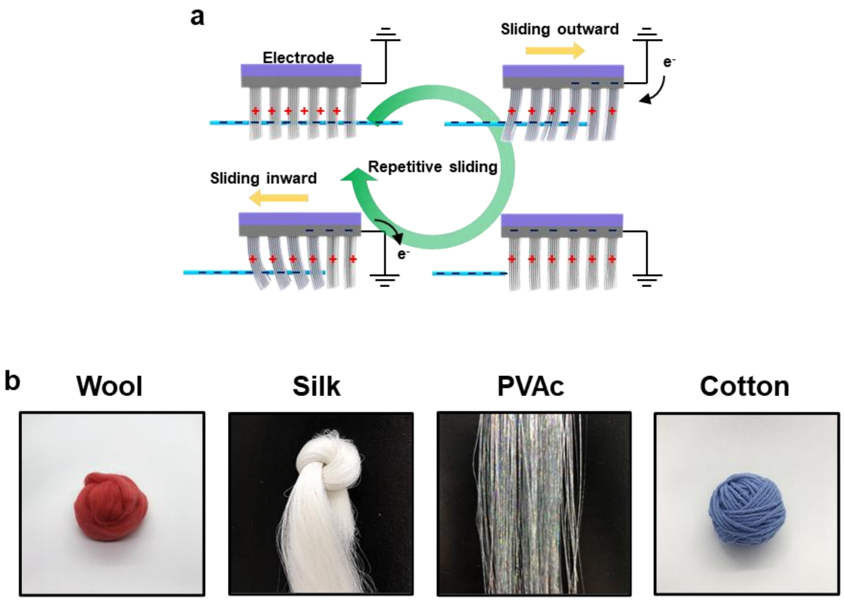

Figure S7. a) The series of schematic illustrations of the related charge transfer mechanism in the single-electrode mode of the TENG. When the MB-TENG is in complete contact with the aligned fibers (i.e., counter material), electrons are injected from the nylon microbrushes to the fibers. As the positively charged nylon microbrushes separate from the negatively charged aligned fibers, a potential difference can be created between them. This potential difference induces the electrons to flow from the ground to the electrode until the microbrushes are completely separated to maintain potential balance. By the nylon microbrushes coming into contact again with aligned fibers, the positive charge induced in the nylon microbrushes decreases. In the following, the accumulated electrons can flow from the electrode to the ground until the electrostatic equilibrium of the two materials is reestablished. b) Photographs of four different fibers (i.e., wool, silk, PVAc, and cotton) used in the regularly aligned fabrics for the horizontal sliding mode.

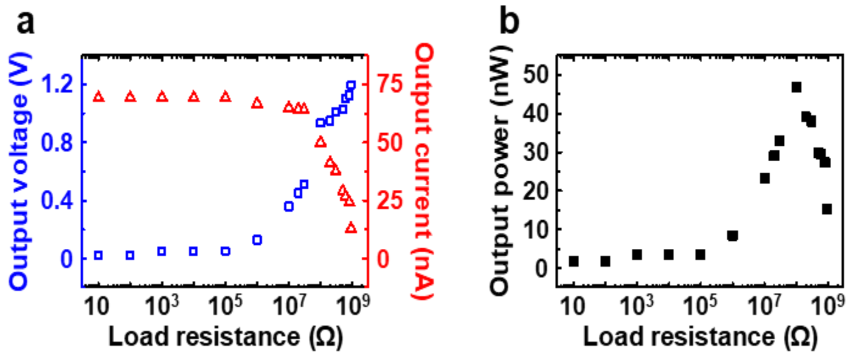

Figure S8. a) The output voltage and current, and b) the output power (i.e., 46.72 nW at 108 Ω) according to the load resistance in the contact-separation mode of the MB-TENG on the PTFE material using a linear motor.

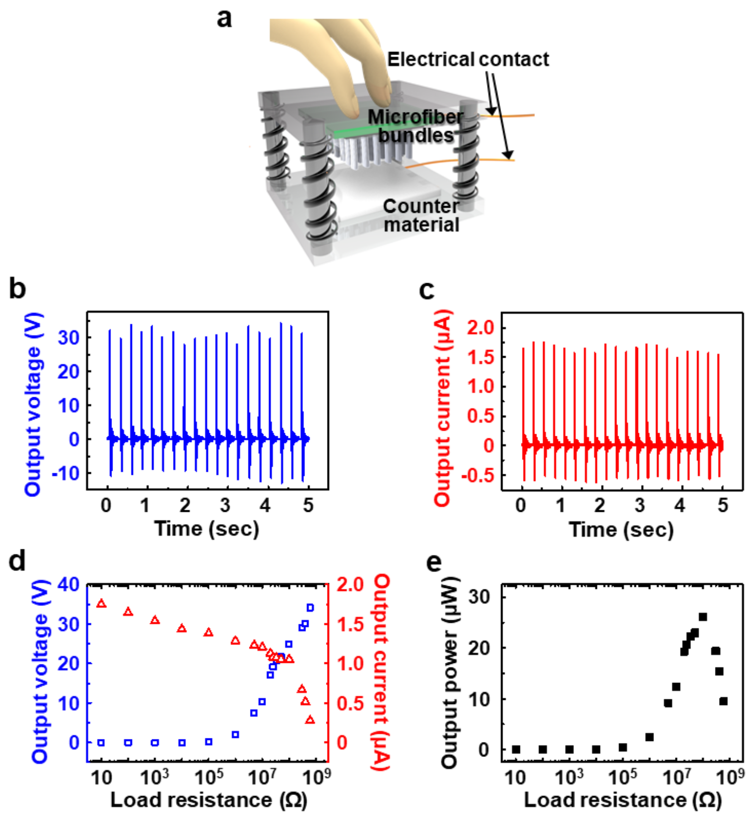

Figure S9. a) A schematic illustration of the hand-tapping contact-separation test on the MB-TENG equipped with the spring-spacer configuration. b-c) The output voltage and current of the MB-TENG with PVC counter material. d) The output voltage and current, and e) the output power of the MB-TENG (i.e., 26.16 μW at 100 MΩ) measured at different external load resistances.

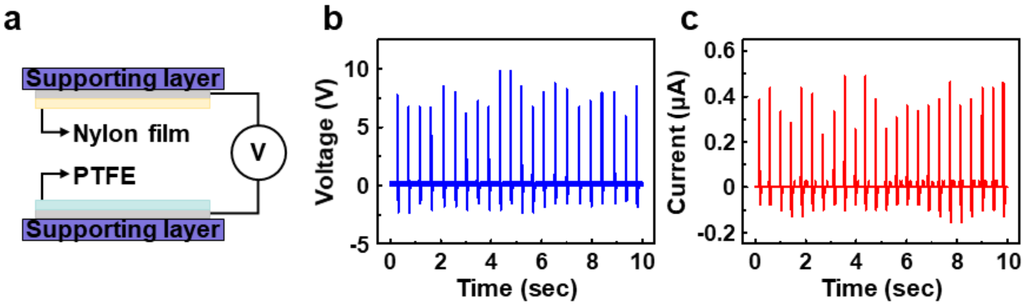

Figure S10. a) A schematic diagram of the hand-tapping test with nylon film. b-c) The output voltage and current in the contact-separation mode using nylon/PTFE films. The actual test area was the same as in the case of the MB-TENG-based module (i.e., 2 × 2 cm^2). Compared with the microfiber test structure, lower output values were found due to the little effect of the increased contact surface area.

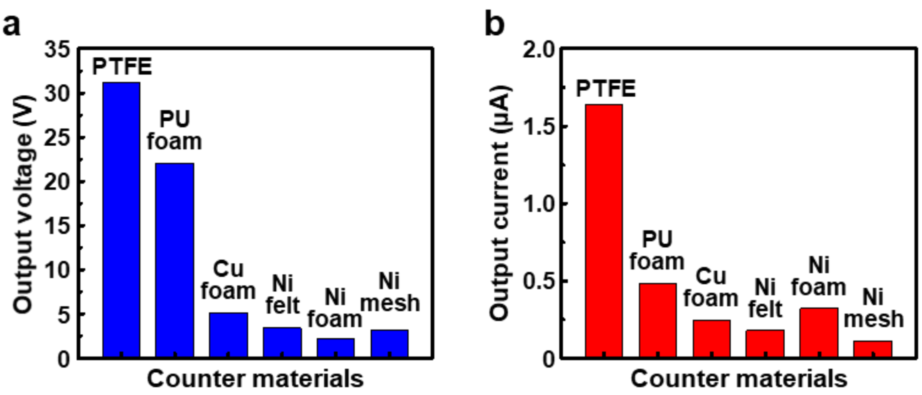

Figure S11. The contact-separation test based on hand-tapping with a variety of counter materials. a-b) The levels of the output voltage and current; the results generally follow the triboelectric series, but in the structure of metal foam, the difference in output values occurred mainly due to the physical deformation of the counter materials by the repeated external force.

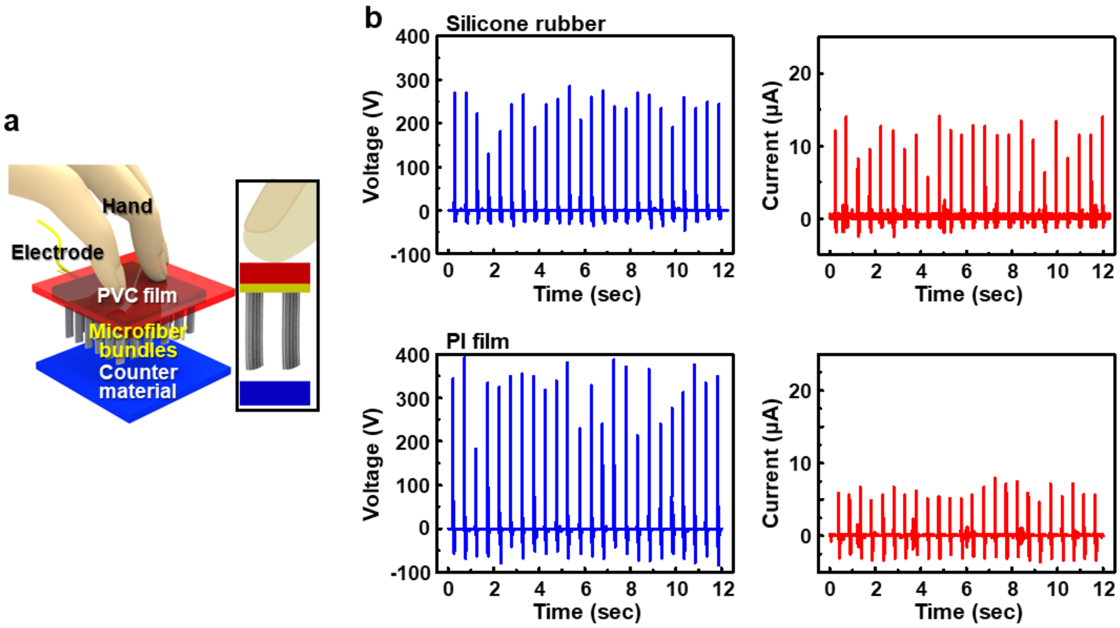

Figure S12. a) A schematic illustration of the PVC film layer-added MB-TENG by covering the top surface of the frame structure in a hand-tapping operation. b) The levels of the output voltage and current when testing silicone rubber and PI film. The performance of the MB-TENG module can be further enhanced by the additional triboelectrification between the PVC film and the human skin (i.e., hand) besides the frictional charge caused by the contact between the microfiber bundles and the counter material in the contact-separation mode, resulting in much higher levels of the output voltage and current as high as ~210, 350 V and 10, 5 µA, respectively.

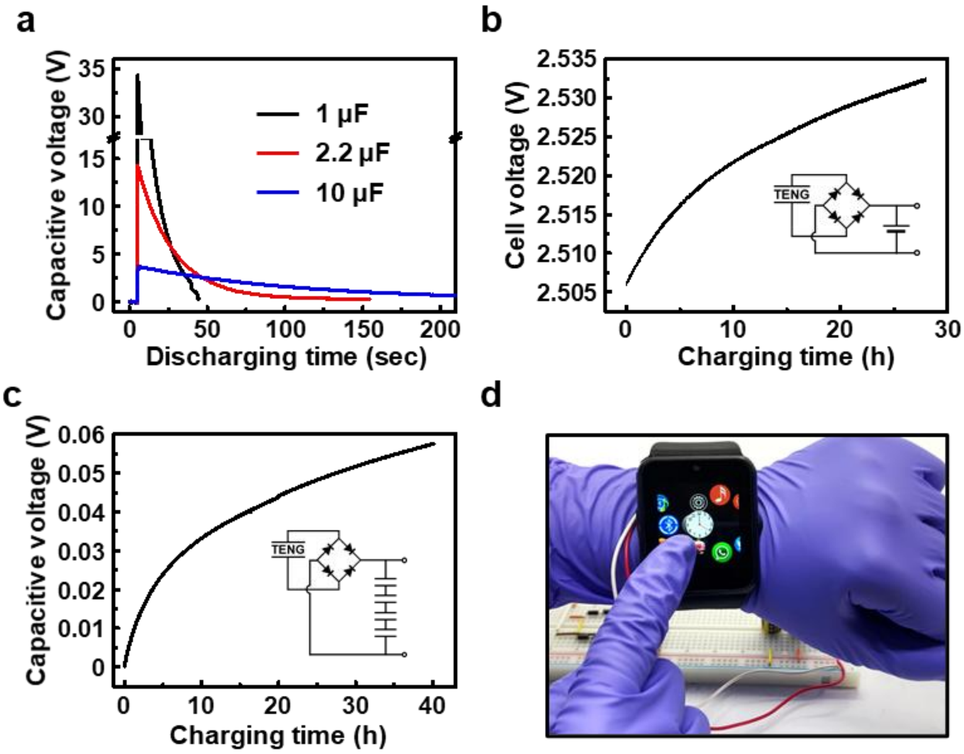

Figure S13. a) An application of the MB-TENG module (see Figure S12) for the fast charge/discharge process (i.e., 1 min) using 1, 2.2, and 10 μF capacitors by the hand-tapping operation in the contact-separation mode; for the 1 min charging process, capacitive voltages reached up to ~34.34, 14.34, and 3.75 V. b) A demonstration of the charging performance for a lithium-ion battery (coin cell, 3 V, 25 mAh) in sliding mode using a linear motor with a bridge-rectifier circuit; the graph represents ~30 mV charging for 30 h. c) A demonstration of the charging performance in sliding mode using a linear motor, in which commercial supercapacitors (i.e., 3.0 V, 10 F) were utilized and serially connected to a bridge-rectifier circuit (inset). d) Real photograph of operating a smartwatch by the charged 2-serial supercapacitors. These demonstrations show that it takes a relatively long time to charge the voltage levels required for a large-scale device operation, but the MB-TENG charged lithium-ion battery and supercapacitors can be applicable to a small-scale device such as a wireless EMG and smartwatch.